**Proceedings of the ASME 2009 International Design Engineering Technical Conferences &
Computers and Information in Engineering Conference
IDETC/CIE 2009
August 30-September 2, 2009, San Diego, USA**

DETC2009-87198

LOCOMOTION OF A SUBMERGED COSSERAT BEAM

Sigrid Leyendecker*
Biocomputing Group
Department of Mathematics and Computer Science
Free University of Berlin
14195 Berlin, Germany
sleye@zedat.fu-berlin.de

Eva Kanso
Dynamical systems, animal hydrodynamic propulsion
Department of Aerospace and Mechanical Engineering
University of Southern California
Los Angeles, California 90089-1453
kanso@usc.edu

ABSTRACT

We study the dynamics and locomotion of a neutrally-buoyant deformable body that can undergo finite *shape deformations and is immersed in a perfect and incompressible fluid. We model the body as a constrained Cosserat beam, more precisely, a Kirchhoff beam, and we derive the equations governing its motion in potential flow where the ambient fluid is accounted for using the added mass effect. We show that the submerged beam can undergo net locomotion due to applied torsional loading on its centerline.*

1 INTRODUCTION

Early efforts in developing mathematically-sound models of swimming can be attributed to the work of Lighthill and Wu, see, e.g., [1, 2]. Interest re-emerged over the past few years to understand the mechanics of fish swimming and thereby enable novel engineering applications such as the design of biologically-inspired vehicles. A model for fish swimming is presented in [3] where the fish is considered to be an articulated body whose shape (i.e., the relative angles between the links forming the articulated body) is controlled or given as a function of time. The internal work required for the body to perform such deformations was neglected. However, it is known that the fish body provides considerable resistance to bending and evidence exists that the elastic properties of the fish body are tuned to hydrodynamic forces (see, e.g., [4–7]).

In this paper, we model the effect of the internal resistance to bending using a Cosserat beam theory with uniform bending rigidity (see [8] for an alternative model) and hyperelastic material behavior (see, e.g., [9]). More precisely, we use a Kirchhoff beam to model the fish, since it fulfils the condition of constant volume automatically. We assume that the beam is submerged in an infinite volume of inviscid, incompressible fluid. A reduced formulation of the dynamics of the beam that does not explicitly incorporate the ambient fluid is derived. The underlying assumption is that the motion of the beam does not generate circulation in the fluid. This formulation is most suited for the analysis of aquatic animals that move at large Reynolds numbers with propulsive movements analogous to those of carangiform and thunniform fish (which move by deforming their bodies in the direction transverse to their swimming motion). Fish can regulate their buoyancy and remain approximately neutrally buoyant when swimming in a plane perpendicular to the direction of gravity. Hence, it is a reasonable first step to model the fish as a neutrally buoyant beam.

The organization of this paper is as follows. We present the Cosserat beam model in Section 2 and the fluid model in Section 3. In Section 4, we discretize the beam and derive an expression for the kinetic energy of the fluid in terms of the *added masses* and the configuration and velocity variables of the discretized beam. In Section 5, we consider planar motions of the beam and in Section 6 we discuss swimming motions of the planar beam subject to prescribed torsional loading on its centerline. The main findings are summarized in Section 7.

*Address all correspondence to this author.

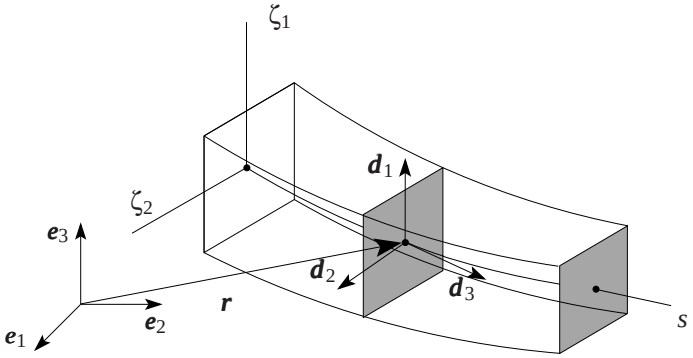

Figure 1. CONFIGURATION OF A BEAM WITH RESPECT TO AN ORTHONORMAL FRAME $\{\boldsymbol{e}_I\}$ FIXED IN SPACE.

2 COSSERAT BEAM

The description of geometrically exact Cosserat beams relies on the kinematic assumption illustrated in Fig. 1, that the placement of a material point in the inertial frame $\{\boldsymbol{e}_I\}$, which is identified by its position vector $\boldsymbol{X}(\zeta_i) \in \mathcal{B}_0 \subset \mathbb{R}^3$ in the reference configuration $\mathcal{B}_0$, can be described by

$$\boldsymbol{x}(\zeta_i, s, t) = \boldsymbol{r}(s,t) + \zeta_i \boldsymbol{d}_i(s,t) \tag{1}$$

see, e.g., [9] or [10]. Note that the sum over the repeated index comprises $i = 1,2$ and the spatial extension of the beam in the longitudinal direction is accounted for by the parametrisation in s. Here $(\zeta_1, \zeta_2, \zeta_3 = s) \in \mathbb{R}^3$ is a triple of curvilinear coordinates with $s \in [0, L] \subset \mathbb{R}$ being the arc-length of the line of centroids $\boldsymbol{r}(s,0) \in \mathbb{R}^3$ in the reference configuration. $\{\boldsymbol{d}_I\}$ represent an orthonormal triad. The directors $\boldsymbol{d}_i(s,t), i = 1,2$, span a principal basis of the cross-section at s and time t which is accordingly assumed to stay planar for all time. In the reference configuration, $\boldsymbol{d}_3$ is tangent to the central line $\boldsymbol{r}(s,0)$ but this is not necessary in a deformed configuration. This allowance of transverse shear deformation corresponds to the Timoshenko beam theory. The beam's configuration variable $\boldsymbol{q}(s,t) = [\boldsymbol{r}(s,t), \boldsymbol{d}_1(s,t), \boldsymbol{d}_2(s,t), \boldsymbol{d}_3(s,t)]^T \in \mathbb{R}^{12}$ is subject to six orthonormality constraints for the director triad.

$$\boldsymbol{d}_i \cdot \boldsymbol{d}_j = \delta_{ij} \tag{2}$$

Therefore, their velocity reads

$$\dot{\boldsymbol{d}}_i = \boldsymbol{\omega} \times \boldsymbol{d}_i,$$

whereby the angular velocity vector $\boldsymbol{\omega}$ can be represented as

$$\boldsymbol{\omega} = \omega_i \boldsymbol{d}_i, \qquad \omega_i = \frac{1}{2} \varepsilon_{ijk} \dot{\boldsymbol{d}}_j \cdot \boldsymbol{d}_k. \tag{3}$$

The strain energy density function $W(\boldsymbol{\Gamma}, \boldsymbol{K})$ is expressed in terms of the objective strain measures

$$\begin{aligned} \boldsymbol{\Gamma}(\boldsymbol{q}) &= \Gamma_i \boldsymbol{e}_i, \quad \Gamma_i = \boldsymbol{d}_i \cdot \frac{\partial \boldsymbol{r}}{\partial s} - \delta_{i3}, \\ \boldsymbol{K}(\boldsymbol{q}) &= K_i \boldsymbol{e}_i, \quad K_i = \frac{1}{2} \varepsilon_{ijk} \left(\boldsymbol{d}_k \cdot \frac{\partial \boldsymbol{d}_j}{\partial s} - (\boldsymbol{d}_k \cdot \frac{\partial \boldsymbol{d}_j}{\partial s})|_{t=0} \right), \end{aligned} \tag{4}$$

where δ_{ij} is the Kronecker delta and ε_{ijk} the alternating symbol. An interpretation of these strain measures can be found in [9], whereupon Γ_1 and Γ_2 measure shear strains, Γ_3 elongation, K_1 and K_2 quantify flexure and K_3 torsion. The constitutive equations

$$\boldsymbol{\nu} = \frac{\partial W}{\partial \boldsymbol{\Gamma}}, \qquad \boldsymbol{\mu} = \frac{\partial W}{\partial \boldsymbol{K}}$$

define the resulting shear forces ν_1, ν_2 and axial force ν_3 and the resulting bending momenta μ_1, μ_2 and torsional moment μ_3 respectively.

The kinetic energy $T_{\mathcal{B}}$ of the deformable body is independent of $\dot{\boldsymbol{d}}_3$. This can be readily verified by differentiating Eqn. (1) in time and noting that the sum over the repeated index comprises $i = 1,2$. The kinetic energy $T_{\mathcal{B}}$ can be written as

$$T_{\mathcal{B}} \;=\; \frac{1}{2} \int_{s=0}^{s=l} \left(\dot{\boldsymbol{r}} \cdot (\rho_{\mathcal{B}} A) \dot{\boldsymbol{r}} + \dot{\boldsymbol{d}}_1 \cdot (\rho_{\mathcal{B}} I_1) \dot{\boldsymbol{d}}_1 + \dot{\boldsymbol{d}}_2 \cdot (\rho_{\mathcal{B}} I_2) \dot{\boldsymbol{d}}_2 \right) ds, \tag{5}$$

where $\rho_{\mathcal{B}}$ is the density of the body (assumed to be uniform), A is the cross-sectional area, I_1 and I_2 are the area moments of inertia of the cross-section.

Kirchhoff beam theory is a special case of the geometrically exact Cosserat beam theory which assumes that the beam is unshearable and inextensible, thus it undergoes pure bending and torsion and $\boldsymbol{\Gamma}$ defined in Eqn. (4) is constrained to be zero everywhere at all times. This is equivalent to the condition that

$$\boldsymbol{d}_3 = \frac{\partial \boldsymbol{r}}{\partial s} \tag{6}$$

is the unit tangent to the centerline. Together with Eqn. (2), the contraint Eqn. (6) accounts for no shear and no elongation.

3 INVISCID AND INCOMPRESSIBLE FLUID

The fluid region $\mathcal{F}$ around the beam is connected. Assume the flow due to deformations of the beam to be irrotational and to have zero circulation. The fluid velocity field $\boldsymbol{u}$ can then be written as the gradient of a potential function ϕ,

$$\boldsymbol{u} \;=\; \nabla \phi. \tag{7}$$

Incompressibility implies that the Laplacian of ϕ is zero,

$$\Delta\phi \;=\; \nabla\cdot(\nabla\phi) \;=\; 0. \tag{8}$$

The impermeability boundary condition on the beam's boundary $\partial\mathcal{B}$ and the condition of zero velocity at infinity can be written as

$$(\nabla\phi)\cdot\boldsymbol{n}\,|_{\partial\mathcal{B}} = (\dot{\boldsymbol{r}}+\zeta_i\dot{\boldsymbol{d}}_i)\cdot\boldsymbol{n}\big|_{\partial\mathcal{B}}\,, \qquad \nabla\phi|_\infty = 0, \tag{9}$$

where $\boldsymbol{n}$ is the unit normal into the fluid.

The kinetic energy of the fluid $T_{\mathcal{F}}$ is given in spatial representation by

$$T_{\mathcal{F}} \;=\; \frac{1}{2}\int_{\mathcal{F}} \rho_{\mathcal{F}}\, \boldsymbol{u}\cdot\boldsymbol{u}\,\mathrm{dv}, \tag{10}$$

where dv the standard volume element on $\mathbb{R}^3$. The Kinetic energy of the fluid Eqn. (10) can be expressed as a boundary integral. First substitute Eqn. (7) into Eqn. (10) and use the identity

$$\mathrm{div}(\phi\nabla\phi) \;=\; \nabla\phi\cdot\nabla\phi+\phi\,\triangle\,\phi$$

together with Eqn. (8). Then, invoke Green's theorem, taking into consideration that the fluid is at rest at infinity Eqn. (23), to get

$$T_{\mathcal{F}} \;=\; \frac{1}{2}\int_{\partial\mathcal{B}} \rho_{\mathcal{F}}\,\phi(\nabla\phi\cdot\boldsymbol{n})\,\mathrm{d}a \;\approx\; \frac{1}{2}\int_{s=0}^{l} \rho_{\mathcal{F}}\,\phi(\nabla\phi\cdot\boldsymbol{n})\,\mathrm{d}s, \tag{11}$$

where $\rho_{\mathcal{F}}$ is the mass density of the fluid and da an infinitesimal area element of $\partial\mathcal{B}$. Note that the integral over the fluid domain in Eqn. (10) reduces to an integral over the boundary of the body $\partial\mathcal{B}$ as shown in the first equality. Given that the cross-sectional dimensions of the submerged body is assumed to be small relative to its length, one could think of the velocity potential ϕ as primarily dependent on the arclength s and time t such that the boundary integral can be approximated as an integral over the centerline of the body as proposed by the last term of Eqn. (11). This approximation is consistent with the Cosserat beam theory employed in Section 2. It is convenient for rewriting the kinetic energy $T_{\mathcal{F}}$ of the fluid in Section 4 as a function of the configuration and velocity of the deformable beam to introduce $\boldsymbol{\varphi}$ and $\boldsymbol{\chi}$ such that

$$\phi = \boldsymbol{\varphi}\cdot\dot{\boldsymbol{r}}+\boldsymbol{\chi}\cdot\boldsymbol{\omega}, \tag{12}$$

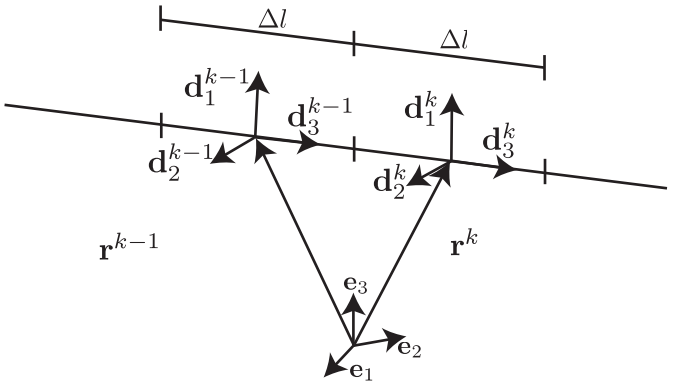

Figure 2. ELEMENT-BASED KIRCHHOFF BEAM.

where $\boldsymbol{\omega}$ is given by Eqn. (3) and $\boldsymbol{\varphi}$, $\boldsymbol{\chi}$ are both vector-valued functions of arclength s and time t. It is worth noting that the virtual linear and angular momenta of the body due to the presence of the surrounding fluid can be defined as follows (see, e.g., [11]),

$$\boldsymbol{p}_{\text{fluid}} = \int_{s=0}^{l} \rho_{\mathcal{F}}\,\phi\,\boldsymbol{n}\,\mathrm{d}s, \qquad \boldsymbol{\pi}_{\text{fluid}} = \int_{s=0}^{l} \rho_{\mathcal{F}}\,\phi\,(\boldsymbol{r}\times\boldsymbol{n})\,\mathrm{d}s, \tag{13}$$

where the angular momentum $\boldsymbol{\pi}_{\text{fluid}}$ is taken about the origin of the inertial frame. One could substitute Eqn. (12) into Eqn. (13) to get

$$\boldsymbol{p}_{\text{fluid}} = \int_0^l \rho_{\mathcal{F}}\,(\boldsymbol{\varphi}\otimes\boldsymbol{n})\cdot\dot{\boldsymbol{r}}\,\mathrm{d}s + \int_0^l \rho_{\mathcal{F}}\,(\boldsymbol{\chi}\otimes\boldsymbol{n})\cdot\boldsymbol{\omega}\,\mathrm{d}s,$$

$$\boldsymbol{\pi}_{\text{fluid}} = \int_0^l \rho_{\mathcal{F}}\,(\boldsymbol{\varphi}\otimes(\boldsymbol{r}\times\boldsymbol{n}))\cdot\dot{\boldsymbol{r}}\,\mathrm{d}s + \int_0^l \rho_{\mathcal{F}}\,(\boldsymbol{\chi}\otimes(\boldsymbol{r}\times\boldsymbol{n}))\cdot\boldsymbol{\omega}\,\mathrm{d}s, \tag{14}$$

where $\rho_{\mathcal{F}}\,(\boldsymbol{\varphi}\otimes\boldsymbol{n})$, $\rho_{\mathcal{F}}\,(\boldsymbol{\chi}\otimes\boldsymbol{n})$, $\rho_{\mathcal{F}}\,(\boldsymbol{\varphi}\otimes(\boldsymbol{r}\times\boldsymbol{n}))$ and $\rho_{\mathcal{F}}\,(\boldsymbol{\chi}\otimes(\boldsymbol{r}\times\boldsymbol{n}))$ are referred to as *added mass per unit length*. A similar expression for the virtual linear momentum $\boldsymbol{p}_{\text{fluid}}$ can be found in Lighthill's slender body theory (see, e.g., [1]). However, Lighthill only consider the first term in Eqn. $(14)_1$ which means that he completely ignores the rotational motion and the way it couples with the translational motion.

4 DISCRETE BEAM, EXACT FLUID

As a first step towards modeling a submerged deformable body undergoing finite deformations, we use the Kirchhoff model of elastic beams which support only bending and torsional deformations. In this case, the condition of constant volume of the beam is fulfilled automatically. The discrete beam formulation described in the sequel is adapted from [12] and [13]

where one-dimensional finite elements are used to discretize the beam. Due to the midpoint evaluation of the discrete strains in Eqn. (16), our formulation corresponds to linear finite elements and converges quadratically.

The centerline of the beam is discretized using $N+1$ points that divide it into N elements or edges of equal length Δl, see Fig. 2. Let $\boldsymbol{q}(t) \in \mathbb{R}^{12N}$ denote the corresponding spatially discrete configuration variable

$$\begin{aligned}\boldsymbol{q}(t) &= \left[\boldsymbol{q}^1(t),\ldots,\boldsymbol{q}^N(t)\right]^T \\ &= \left[\boldsymbol{r}^1(t),\boldsymbol{d}_1^1(t),\boldsymbol{d}_2^1(t),\boldsymbol{d}_3^1(t),\ldots,\boldsymbol{r}^N(t),\boldsymbol{d}_1^N(t),\boldsymbol{d}_2^N(t),\boldsymbol{d}_3^N(t)\right]^T,\end{aligned}$$

where $\boldsymbol{r}^k$ denotes the placement of the k-th element center and the director triad $\{\boldsymbol{d}_I^k\}$ represents its orientation in space. $\boldsymbol{q}(t)$ is subject to the orthonormality constraints Eqn. (2) for each triad. Additionally, unshearability and inextensibilty give rise to the constraints

$$\boldsymbol{r}^k = \boldsymbol{r}^{k-1} + \frac{\Delta l}{2}\left(\boldsymbol{d}_3^{k-1} + \boldsymbol{d}_3^k\right) \tag{15}$$

for $k = 2,\ldots,N$. The bending and torsion strains caused by relative rotation of adjacent elements read

$$K_i^{k-1,k} = \frac{1}{2}\varepsilon_{ijl}\left(\frac{\boldsymbol{d}_l^k + \boldsymbol{d}_l^{k-1}}{2}\cdot\frac{\boldsymbol{d}_j^k - \boldsymbol{d}_j^{k-1}}{\Delta l} - K_{i|_{t=0}}^{k-1,k}\right). \tag{16}$$

Assuming that the beam deformations are governed by hyperelastic material behaviour, the stored-energy function takes the form

$$\begin{aligned}W(\boldsymbol{K}) = &\frac{\Delta l}{2}\sum_{k=2}^{N}\left(EI_1^{k-1,k}\left(K_1^{k-1,k}\right)^2 + EI_2^{k-1,k}\left(K_2^{k-1,k}\right)^2\right. \\ &\left. + GJ^{k-1,k}\left(K_3^{k-1,k}\right)^2\right)\end{aligned} \tag{17}$$

with the bending and torsional stiffness $EI_1^{k-1,k}$, $EI_2^{k-1,k}$ and $GJ^{k-1,k}$, respectively. The kinetic energy $T_{\mathcal{B}}$ of Eqn. (5) can be discretized in a straightforward way

$$T_{\mathcal{B}} = \frac{\Delta l}{2}\sum_{k=1}^{N}\left(\dot{\boldsymbol{r}}^k\cdot(\rho_{\mathcal{B}}A)\dot{\boldsymbol{r}}^k + \dot{\boldsymbol{d}}_1^k\cdot(\rho_{\mathcal{B}}I_1)\dot{\boldsymbol{d}}_1^k + \dot{\boldsymbol{d}}_2^k\cdot(\rho_{\mathcal{B}}I_2)\dot{\boldsymbol{d}}_2^k\right). \tag{18}$$

We assume that the spatial discretization of the beam does not correspond to a spatial discretization of the fluid domain. In other words, we consider a discretized beam moving in a spatially-continuous fluid domain so that the gradient and the Laplacian of the fluid potential are meaningful operators. This modeling approach is similar in spirit to that in [3] where the immersed body is discretized into three sections from the onset. The fluid kinetic energy Eqn. (11) can be written as

$$T_{\mathcal{F}} = \frac{1}{2}\int_0^l \rho_{\mathcal{F}}\,\phi(\nabla\phi\cdot\boldsymbol{n})\,\mathrm{d}s \approx \frac{1}{2}\sum_{k=1}^{N}\int_{(k-1)\Delta l}^{k\Delta l}\rho_{\mathcal{F}}\,\phi(\nabla\phi\cdot\boldsymbol{n}^k)\,ds. \tag{19}$$

Our goal is to find an expression for the kinetic energy $T_{\mathcal{F}}$ that is only function of the configuration and velocity of the discretized deformable body. By virtue of the linearity of Laplace's equation, one could apply the principle of superposition to write the potential ϕ as a sum of potential functions

$$\phi = \sum_{i=1}^{N}\phi^i \tag{20}$$

where ϕ^i is the potential function due to a motion of the i^{th} element. That is, ϕ^i is a solution of Laplace's equation subject to the following boundary conditions (no sum on i)

$$\left.\frac{\partial\phi^i}{\partial n^j}\right|_{\partial\mathcal{B}} = \begin{cases}\left.(\dot{\boldsymbol{r}}^i + \zeta_l\dot{\boldsymbol{d}}_l^i)\cdot\boldsymbol{n}^j\right|_{\partial\mathcal{B}} & \text{for } i = j \\ 0 & \text{for } i \neq j\end{cases}, \qquad \left.\nabla\phi^i\right|_{\infty} = 0. \tag{21}$$

The potentials ϕ^i can be written as done in Eqn. (12)

$$\phi^i = \boldsymbol{\varphi}^i\cdot\dot{\boldsymbol{r}}^i + \boldsymbol{\chi}^i\cdot\boldsymbol{\omega}^i \qquad (\text{no sum on } i). \tag{22}$$

Here, $\boldsymbol{\varphi}^k$ and $\boldsymbol{\chi}^k$ are potential functions (of both s and t) subject to proper boundary conditions. These conditions are obtained by substituting Eqn. (22) into Eqn. (21) and using the fact that

$$\boldsymbol{\omega}^i = \boldsymbol{D}_l^i\dot{\boldsymbol{d}}_l^i, \qquad \boldsymbol{D}_l^i = -\frac{1}{2}(\varepsilon_{mnl}\boldsymbol{d}_m^i\otimes\boldsymbol{d}_n^i) \qquad (\text{no sum on } i),$$

and $\boldsymbol{D}_l^i = -\frac{1}{2}(\varepsilon_{mnl}\boldsymbol{d}_m^i\otimes\boldsymbol{d}_n^i)$ is orthogonal (hence its inverse is equal to its transpose). To this end, one gets

$$\left.\frac{\partial\boldsymbol{\varphi}^i}{\partial n^j}\right|_{\partial\mathcal{B}} = \delta^{ji}\boldsymbol{n}^j, \qquad \left.\frac{\partial\boldsymbol{\chi}^i}{\partial n^j}\right|_{\partial\mathcal{B}} = \zeta_l\boldsymbol{D}_l^i(\delta^{ji}\boldsymbol{n}^j)|_{\partial\mathcal{B}} \quad (\text{no sum on } i). \tag{23}$$

Now, substitute Eqn. (22) into Eqn. (20) and use the resulting expression for ϕ in Eqn. (19) to get, upon employing the boundary

conditions Eqn. (23) and simplifying, that

$$T_{\mathcal{F}} = \frac{1}{2}\sum_{i=1}^{N}\sum_{k=1}^{N}\left[\dot{\boldsymbol{r}}^i\cdot\Theta_r^{ik}\dot{\boldsymbol{r}}^k + 2\dot{\boldsymbol{r}}^i\cdot\Theta_{r\omega}^{ik}\boldsymbol{\omega}^k + \boldsymbol{\omega}^i\cdot\Theta_{\omega}^{ik}\cdot\boldsymbol{\omega}^k\right], \quad (24)$$

where

$$\Theta_r^{ik} = \int_{(k-1)\Delta l}^{k\Delta l}\rho_{\mathcal{F}}\,\boldsymbol{\varphi}^i\otimes\boldsymbol{n}^k ds, \qquad \Theta_{\omega}^{ik} = \int_{(k-1)\Delta l}^{k\Delta l}\rho_{\mathcal{F}}\,\boldsymbol{\chi}^i\otimes\zeta_l\boldsymbol{D}_l^k\cdot\boldsymbol{n}^k ds,$$

$$\Theta_{r\omega}^{ik} = \frac{1}{2}\int_{(k-1)\Delta l}^{k\Delta l}\rho_{\mathcal{F}}\left(\boldsymbol{\varphi}^i\otimes\zeta_l\boldsymbol{D}_l^k\cdot\boldsymbol{n}^k + \boldsymbol{\chi}^i\otimes\boldsymbol{n}^k\right)ds. \quad (25)$$

The kinetic energy Eqn. (24) can be rewritten in terms of $\dot{\boldsymbol{q}}^i(t) = \left[\dot{\boldsymbol{r}}^i(t), \dot{\boldsymbol{d}}_1^i(t), \dot{\boldsymbol{d}}_2^i(t), \dot{\boldsymbol{d}}_3^i(t)\right]^T$ in the compact form

$$T_{\mathcal{F}} = \frac{1}{2}\sum_{i=1}^{N}\sum_{k=1}^{N}\dot{\boldsymbol{q}}^i\cdot\mathbb{M}_f^{ik}\cdot\dot{\boldsymbol{q}}^k, \quad (26)$$

where $\mathbb{M}_f^{ik}$ is the *added mass matrix*

$$\mathbb{M}_f^{ik} = \begin{bmatrix} \Theta_r^{ik} & \Theta_{r\omega}^{ik}\boldsymbol{D}_1^k & \Theta_{r\omega}^{ik}\boldsymbol{D}_2^k & \Theta_{r\omega}^{ik}\boldsymbol{D}_3^k \\ (\boldsymbol{D}_1^i)^T\Theta_{r\omega}^{ik} & (\boldsymbol{D}_1^i)^T\Theta_{\omega}^{ik}\boldsymbol{D}_1^k & (\boldsymbol{D}_1^i)^T\Theta_{\omega}^{ik}\boldsymbol{D}_2^k & (\boldsymbol{D}_1^i)^T\Theta_{\omega}^{ik}\boldsymbol{D}_3^k \\ (\boldsymbol{D}_2^i)^T\Theta_{r\omega}^{ik} & (\boldsymbol{D}_2^i)^T\Theta_{\omega}^{ik}\boldsymbol{D}_1^k & (\boldsymbol{D}_2^i)^T\Theta_{\omega}^{ik}\boldsymbol{D}_2^k & (\boldsymbol{D}_2^i)^T\Theta_{\omega}^{ik}\boldsymbol{D}_3^k \\ (\boldsymbol{D}_3^i)^T\Theta_{r\omega}^{ik} & (\boldsymbol{D}_3^i)^T\Theta_{\omega}^{ik}\boldsymbol{D}_1^k & (\boldsymbol{D}_3^i)^T\Theta_{\omega}^{ik}\boldsymbol{D}_2^k & (\boldsymbol{D}_3^i)^T\Theta_{\omega}^{ik}\boldsymbol{D}_3^k \end{bmatrix}.$$

5 TWO-DIMENSIONAL MOTION

Consider a two-dimensional beam in pure bending and write the velocity potentials $\boldsymbol{\varphi}^k$ and $\boldsymbol{\chi}^k$ with respect to the triad attached to element k

$$\boldsymbol{\varphi}^k = \varphi_1^k\boldsymbol{d}_1^k + \varphi_3^k\boldsymbol{d}_3^k, \qquad \boldsymbol{\chi}^k = \chi_2^k\boldsymbol{d}_2^k.$$

Also write the velocity of element k as $\dot{\boldsymbol{r}}^k = (\dot{\boldsymbol{r}}^k\cdot\boldsymbol{d}_1^k)\boldsymbol{d}_1^k + (\dot{\boldsymbol{r}}^k\cdot\boldsymbol{d}_3^k)\boldsymbol{d}_3^k$ and $\boldsymbol{\omega}^k = \omega_2^k\boldsymbol{d}_2^k$ where $\omega_2^k = \frac{1}{2}\varepsilon_{2jl}\dot{\boldsymbol{d}}_j^k\cdot\boldsymbol{d}_l^k = \frac{1}{2}(\dot{\boldsymbol{d}}_3^k\cdot\boldsymbol{d}_1^k - \dot{\boldsymbol{d}}_1^k\cdot\boldsymbol{d}_3^k)$. The unit vector normal to element j is simply $\boldsymbol{n}^j = \boldsymbol{d}_1^j$. The velocity potentials φ_1^k are thus given by the Neumann problem

$$\Delta\varphi_1^k = 0 \quad \text{such that}$$
$$\nabla\varphi_1^k\cdot\boldsymbol{d}_1^j\Big|_{\partial\mathcal{B}} = \delta^{jk}\boldsymbol{d}_1^j\cdot\boldsymbol{d}_1^k = \begin{cases} 1 \text{ for } i=j \\ 0 \text{ for } i\neq j \end{cases}, \qquad \nabla\varphi_1^k\Big|_{\infty} = 0. \quad (27)$$

Similarly, the velocity potentials φ_3^k are given by

$$\Delta\varphi_3^k = 0 \quad \text{such that}$$
$$\nabla\varphi_3^k\cdot\boldsymbol{d}_1^j\Big|_{\partial\mathcal{B}} = \delta^{jk}\boldsymbol{d}_1^j\cdot\boldsymbol{d}_3^k = 0, \qquad \nabla\varphi_3^k\Big|_{\infty} = 0.$$

That is, φ_3^k are identically zero for all time and all k. The velocity potentials χ_2^k are also solutions to Laplace's equations subject to zero decay at infinity and

$$\nabla\chi_2^k\cdot\boldsymbol{d}_1^j\Big|_{\partial\mathcal{B}} = (\zeta_l\boldsymbol{D}_l^k\cdot\delta^{jk}\boldsymbol{d}_1^j)\cdot\boldsymbol{d}_2^k\Big|_{\partial\mathcal{B}} = \begin{cases} \frac{1}{2}s \text{ where } s\in((k-1)\Delta l,\ k\Delta l) & \text{for } k=j \\ 0 & \text{for } k\neq j \end{cases}. \quad (28)$$

Substitute the above expressions for the potentials $\boldsymbol{\varphi}^k$ and $\boldsymbol{\chi}^k$ and the corresponding boundary conditions into Eqn. (25) to get

$$\begin{aligned} &\Theta_r^{ik} = \alpha^{ik}\boldsymbol{d}_1^i\otimes\boldsymbol{d}_1^k, \qquad \Theta_{\omega}^{ik} = \beta^{ik}\boldsymbol{d}_2^i\otimes\boldsymbol{d}_2^k, \\ &\Theta_{r\omega}^{ik} = \gamma^{ik}(\boldsymbol{d}_1^i\otimes\boldsymbol{d}_2^k + \boldsymbol{d}_2^i\otimes\boldsymbol{d}_1^k), \end{aligned} \quad (29)$$

where

$$\alpha^{ik} = \int_{(k-1)\Delta l}^{k\Delta l}\rho_{\mathcal{F}}\,\varphi_1^i ds, \qquad \beta^{ik} = \int_{(k-1)\Delta l}^{k\Delta l}\frac{1}{2}\rho_{\mathcal{F}}\,\chi_2^i s\,ds,$$

$$\gamma^{ik} = \frac{1}{2}\int_{(k-1)\Delta l}^{k\Delta l}\frac{1}{2}\rho_{\mathcal{F}}\,\varphi_1^i s\,ds = \frac{1}{2}\int_{(k-1)\Delta l}^{k\Delta l}\rho_{\mathcal{F}}\,\chi_2^i ds.$$

By virtue of Eqn. (29) and using Eqn. $\boldsymbol{\omega}^k = \omega_2^k\boldsymbol{d}_2^k$ where $\omega_2^k = \frac{1}{2}\varepsilon_{2jl}\dot{\boldsymbol{d}}_j^k\cdot\boldsymbol{d}_l^k = \frac{1}{2}(\dot{\boldsymbol{d}}_3^k\cdot\boldsymbol{d}_1^k - \dot{\boldsymbol{d}}_1^k\cdot\boldsymbol{d}_3^k)$, the kinetic energy of the fluid Eqn. (24) and Eqn. (26) can be rewritten in the convenient form

$$T_{\mathcal{F}} = \frac{1}{2}\sum_{i=1}^{N}\sum_{k=1}^{N}\left[\dot{\boldsymbol{r}}^i\ \dot{\boldsymbol{d}}_1^i\ \dot{\boldsymbol{d}}_3^i\right]\cdot\mathbb{M}_f^{ik}\cdot\begin{bmatrix}\dot{\boldsymbol{r}}^k\\ \dot{\boldsymbol{d}}_1^k\\ \dot{\boldsymbol{d}}_3^k\end{bmatrix} \quad (30)$$

with

$$\mathbb{M}_f^{ik} = \begin{bmatrix} \alpha^{ik}\boldsymbol{d}_1^i\otimes\boldsymbol{d}_1^k & -\frac{\gamma^{ik}}{2}\boldsymbol{d}_1^i\otimes\boldsymbol{d}_3^k & \frac{\gamma^{ik}}{2}\boldsymbol{d}_1^i\otimes\boldsymbol{d}_1^k \\ -\frac{\gamma^{ik}}{2}\boldsymbol{d}_3^i\otimes\boldsymbol{d}_1^k & \frac{\beta^{ik}}{4}\boldsymbol{d}_3^i\otimes\boldsymbol{d}_3^k & -\frac{\beta^{ik}}{4}\boldsymbol{d}_3^i\otimes\boldsymbol{d}_1^k \\ \frac{\gamma^{ik}}{2}\boldsymbol{d}_1^i\otimes\boldsymbol{d}_1^k & -\frac{\beta^{ik}}{4}\boldsymbol{d}_1^i\otimes\boldsymbol{d}_3^k & \frac{\beta^{ik}}{4}\boldsymbol{d}_1^i\otimes\boldsymbol{d}_1^k \end{bmatrix}.$$

The total energy of the body-fluid system is obtained by adding the two-dimensional version of Eqn. (18) and Eqn. (30),

$$T = T_{\mathcal{B}} + T_{\mathcal{F}} = \frac{1}{2}\sum_{i=1}^{N}\sum_{k=1}^{N} \dot{\boldsymbol{q}}^i \cdot (\delta^{ik}\mathbb{M}_b^k + \mathbb{M}_f^{ik}) \cdot \dot{\boldsymbol{q}}^k. \qquad (31)$$

The constant mass tensors $\mathbb{M}_b^k$ are given by

$$\mathbb{M}_b^k = \Delta l \begin{bmatrix} (\rho_{\mathcal{B}} A)\boldsymbol{I} & \boldsymbol{0} & \boldsymbol{0} \\ \boldsymbol{0} & (\rho_{\mathcal{B}} I_1)\boldsymbol{I} & \boldsymbol{0} \\ \boldsymbol{0} & \boldsymbol{0} & \boldsymbol{0} \end{bmatrix}, \qquad (32)$$

where $\boldsymbol{I}$ and $\boldsymbol{0}$ denote the 2×2 identity and zero matrix, respectively. Furthermore, in the two-dimensional case only bending with respect to the out of plane axis occurs and the stored energy function given in Eqn. (17) reduces to

$$W(\boldsymbol{K}) = \frac{\Delta l}{2}\sum_{k=2}^{N} EI^{k-1,k}\left(K_2^{k-1,k}\right)^2. \qquad (33)$$

6 LOCOMOTION OF THE SUBMERGED BEAM

Numerical method

The problem of solving Laplace's equation for the velocity potentials over the fluid domain $\mathcal{F}$ subject to zero velocity at infinity and impermeable boundary conditions can be done numerically using a *boundary element method*, also referred to as a panel method. We use the panel method devised by [14] (see also [15]) which utilizes a piecewise-constant distribution of *source singularities* over the boundary of the submerged body and computes the strength of this distribution by imposing appropriate boundary conditions. The use of source/sink distributions cannot contribute any net circulation around the body and allows one to ensure a priori that the circulation in the fluid remains zero at all time. Physically speaking, this *fictitious source distribution* induces a velocity field in the fluid that is equivalent to the velocity field resulting from the motion of the submerged body. The theoretical foundation of such panel methods is based on reformulating Laplace's equations as a boundary integral equation, using the divergence theorem, see, e.g., [16](Chapter 6).

For the submerged planar Cosserat beam, we solve for $2N$ distinct source distributions corresponding to the $2N$ velocity potentials φ_1^k, χ_2^k $(k = 1,\ldots,N)$ subject to the two sets of boundary conditions in Eqn. (27) and Eqn. (28).

Time-integration of the equations of motion is performed with a *variational integrator*, see, e.g., [17], yielding a symplectic-momentum conserving discrete trajectory. Details on variational integrators for constrained systems can be found in [18]. Accordingly, using *Lagrange multipliers* $\boldsymbol{\lambda}$ to enforce the holonomic constraints Eqn. (2) and Eqn. (15) combined in $\boldsymbol{g}(\boldsymbol{q}) = \boldsymbol{0}$, the constrained discrete Euler-Lagrange equations take the form

$$\begin{aligned} D_1L_d(\boldsymbol{q}_n,\boldsymbol{q}_{n+1}) + D_2L_d(\boldsymbol{q}_{n-1},\boldsymbol{q}_n) - \Delta t\boldsymbol{G}^T(\boldsymbol{q}_n)\cdot\boldsymbol{\lambda}_n &= \boldsymbol{0} \\ \boldsymbol{g}(\boldsymbol{q}_{n+1}) &= \boldsymbol{0} \end{aligned} \qquad (34)$$

Here, Δt denotes the time-step and L_d is the discrete Lagrangian which approximates the action integral of the continuous Lagrangian L over one time interval. Specifically, we use $L = T - W$, where T is given in (31) and W is given in (33) and discretize in time using the approximation

$$\begin{aligned} L_d(\boldsymbol{q}_n,\boldsymbol{q}_{n+1}) = &\frac{1}{2\Delta t}(\boldsymbol{q}_{n+1}-\boldsymbol{q}_n)\cdot(\mathbb{M}_b + \mathbb{M}_f(\boldsymbol{q}_n))\cdot(\boldsymbol{q}_{n+1}-\boldsymbol{q}_n) \\ &- \Delta t W(\boldsymbol{K}(\boldsymbol{q}_{n+\frac{1}{2}})) \end{aligned}$$

where $\boldsymbol{q}_{n+\frac{1}{2}}$ denotes the midpoint of $\boldsymbol{q}_n$ and $\boldsymbol{q}_{n+1}$. In the regime of finite (geometrically nonlinear) elastic deformations that we consider here, the midpoint evaluation of the stored energy function enhances the robustness of the simulation, compared to the evaluation $W(\boldsymbol{K}(\boldsymbol{q}_n))$ at the last time-node, and substantially larger time-steps can be used. The resulting implicit time-stepping scheme Eqn. (34) is solved using Newton-iteration.

This discrete Lagrangian is invariant with respect to rigid body motion superposed on the beam configuration. Due to the variational nature of the time-stepping scheme, the corresponding discrete momentum maps, namely the total linear and angular momentum of the fluid-solid-system are exactly conserved (up to the numerical tolerance of 10^{-9} employed in the Newton-iteration). Furthermore, solution shows the typical good energy behaviour of variational integrators in the sense that that total energy of the fluid-solid-system is oscillating with small amplitude, in particular, energy is not gained or dissipated numerically.

Numerical examples and discussion

In the sequel, different types of 'swimming' resulting from different loading, stiffness, geometry, discretization and initial condition are discussed. The focus is on the locomotion of the 'fish' rather than on the beam deformation. Table 1 summarises the parameter values in the different simulations. All dynamic simulations are based on the constant time-step $\Delta t = 10^{-2}$, the fluid density $\rho_{\mathcal{F}} = 10$ and the inertia parameters of the beam $(\rho_{\mathcal{B}} A) = 3.1\cdot 10^{-1}$ and $(\rho_{\mathcal{B}} I_1) = 7.8\cdot 10^{-6}$ appearing in the constant mass matrix of the beam Eqn. (32). In general, the number of fluid panels per element is 4, except when very coarse discretizations are used, e.g. $N = 3$, then it is increased to 12. Furthermore, the loading torques vary according to $\tau(t,s) = A\cos(ft - \kappa s/l)$ with $f = \kappa = 2\pi$ in time and space, see Fig. 3.

Table 1. PARAMETER VALUES IN THE DIFFERENT SIMULATIONS.

i)	$\Delta t = 10^{-2}$s	$\rho_{\mathcal{F}} = 10$kg/m^3			
⋮	$(\rho_{\mathcal{B}} A) = 3.1 \cdot 10^{-1}$kg/m	$(\rho_{\mathcal{B}} I_1) = 7.8 \cdot 10^{-6}$kg/m			
xii)	$f = \kappa = 2\pi$				
	A	EI[Nm^2]	l[m]	N	$\boldsymbol{v}_0$[m/s]
i)	1	5	1	9	$[0,0]$
ii)	1	10	1	9	$[0,0]$
iii)	0.5	5	1	9	$[0,0]$
iv)	1	5	1	3	$[0,0]$
v)	0.5	5	2	9	$[0,0]$
vi)	1	$[5,50]$	1	9	$[0,0]$
vii)	1	$[3,10]$	1	9	$[0,0]$
viii)	$[0,1]$	5	1	9	$[0,0]$
ix)	$[0,1]$	5	1	9	$[0,0]$
x)	0	5	1	3	$[10^{-1},10^{-4}]$
xi)	0	5	1	9	$[10^{-1},10^{-4}]$
xii)	0	5	1	27	$[10^{-1},10^{-4}]$

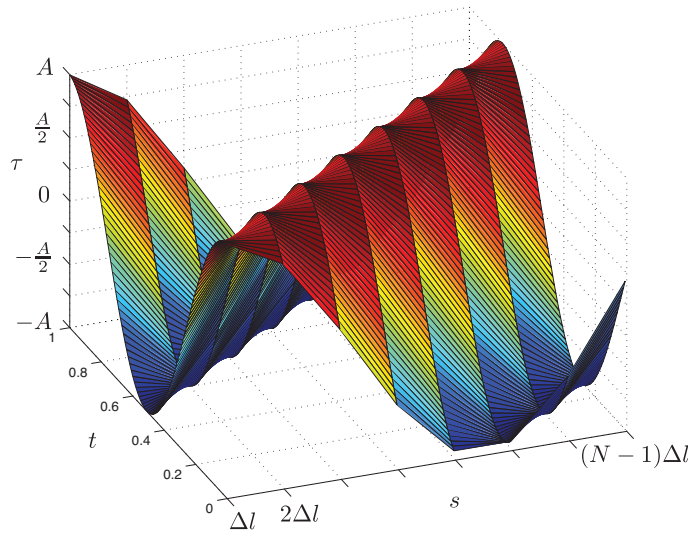

Figure 3. APPLIED TORQUES BETWEEN THE ELEMENTS $\tau(t,s) = A\cos(ft - \kappa s/l)$ WITH $f = \kappa = 2\pi$.

Active swimming refers to the case where the beam undergoes a net locomotion due to prescribed loading on its centerline. We think of the prescribed loading as the activation mechanism which is responsible for locomotion similar to the muscle activation in real fish. During active swimming, nonzero torques are applied at the 'joints' between the elements.

Fig. 4 shows the trajectories of three different simulations. In each element's center, the two directors are attached to illustrate the element's orientation. While showing the same qualitative motion, namely swimming to the left and performing a slight curve to the right, clearly, the trajectories as well as the swimming velocity depend in a nontrivial way on the beam parameters as well as the loading. In the top simulation *i*), the ratio between the beam's stiffness and the amplitude of the loading leads to faster swimming motion in comparison to *ii*) and *iii*). In *ii*), the same loading is applied to the twice as stiff beam which leads to smaller deformation and results in slower motion. In the bottom simulation *iii*), the stiffness is equal to that in *i*), however the amplitude of the loading is only half as big leading to even slower motion.

Using a coarse spatial discretization yields a less stable motion (see also below for a discussion of the relation between the discretization and stability). Trajectory *iv*) in Fig. 5 passes trough a semicircle during the simulation time $t = 100$, while in the same simulation with a finer discretization *i*), the trajectory shows only a slight curve. Remarkably, in simulation *v*), the beam turns to the right trough a quadrant. The beam is twice as long as that in *iii*) and shows a qualitatively different (turning instead of forward motion) and much faster motion.

Two simulations with different bending stiffness varying along the centerline of the beam are shown in Fig. 6. Both beams move to the left and perform slight left curves in contrast to the right curved trajectories of the equally loaded beams in *i*) and *ii*). In the top simulation *vi*), the first half of the beam (the 'head') is ten times stiffer than the second half (the 'tail'). One can observe that bending occurs in the second half of the beam only. The very slow velocity of the motion indicates that being able to bend the head may be important for fast swimming. In comparison to *vi*), the beam in *vii*) moves faster and shows also deformation of the head. Its bending stiffness varies linearly from $EI^{1,2} = 10$ at the head to $EI^{8,9} = 3$ at the tail.

Next, we investigate two kinds of swimming behavior as shown in Fig. 7. First in *viii*), torques are applied between all the elements for a period of $t = 50$, such that until this time, it moves as simulation *i*). After that, the beam undergoes passive swimming and is rapidly slowing down and moves into a tighter curve. Secondly, in *ix*), only the head (the first four elements from the left) is loaded by nonzero torques. This beam moves slowly to the left on an almost straight trajectory.

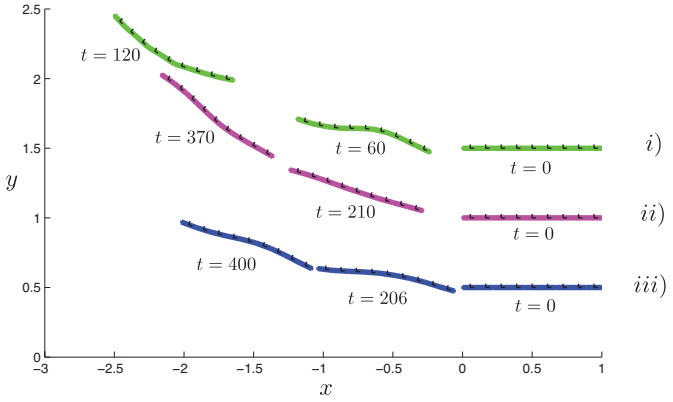

Figure 4. BEAM CONFIGURATIONS WITH DIFFERENT APPLIED TORQUES AND STIFFNESS PARAMETERS, $i)\ A=1, EI=5$, $ii)\ A=1, EI=10$ AND $iii)\ A=0.5, EI=5$.

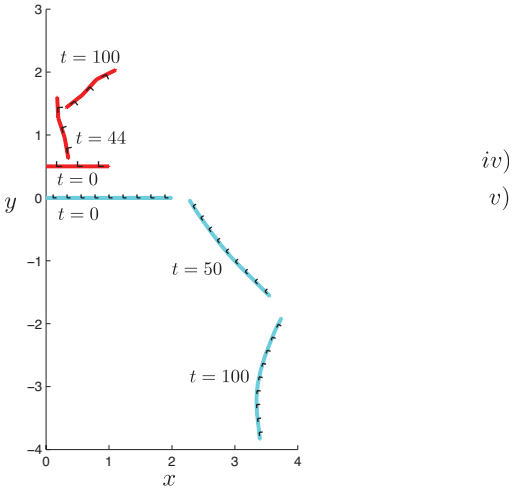

Figure 5. BEAM CONFIGURATIONS WITH DIFFERENT APPLIED TORQUES, LENGTHS AND NUMBER OF ELEMENTS, $iv)\ A=1, l=1, N=3$ AND $v)\ A=0.5, l=2, N=9$.

Finally, we examine the behavior of the beam when it is moving passively with no applied torques. We focus on the case when the beam is given an initial translational velocity along its undeformed length. This motion is a relative equilibrium, that is, in the absence of any loading and disturbances, the beam continues to move with the same translational velocity. We numerically examine the behavior of the beam with no torque loading

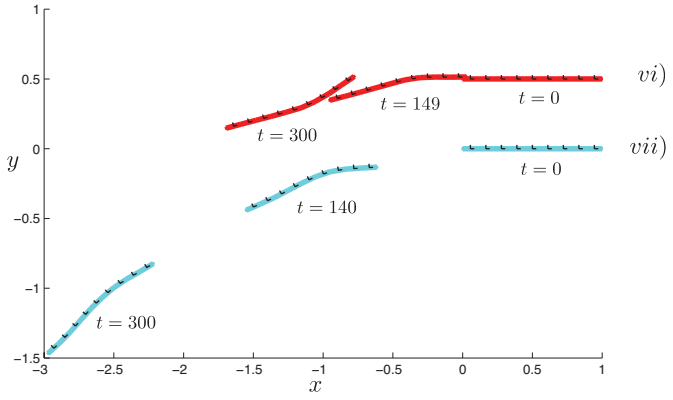

Figure 6. BEAM CONFIGURATIONS WITH DIFFERENT STIFFNESS VARYING ALONG THE BEAM, $xi)\ EI=50, s<\frac{l}{2}, EI=5, s>\frac{l}{2}$ AND $xii)\ EI=11-\frac{s}{\Delta l}$.

but only a given initial velocity. In a first numerical experiment, only a translational initial velocity of $\mathbf{v}_0=[0.1,0]$ in x-direction was imposed on every element and beams consisting of $N=3$ and $N=9$ elements have been tested. Both the coarsely and the finely discretized beams were swimming perfectly stable to the right for $t=100$. In a second experiment, a small perturbation in the initial y-velocity is given and we look for the first occurrence of unstable behavior in the sense that the beam leaves its horizontal configuration (with an end node's y-coordinate devi-

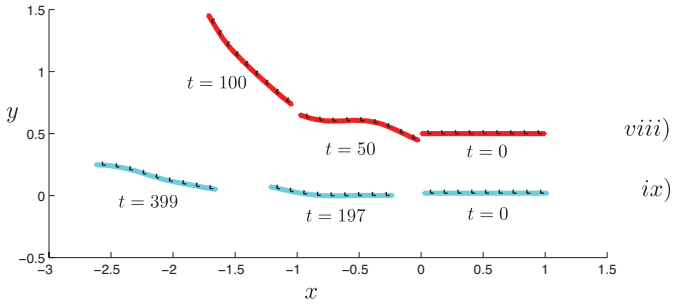

Figure 7. BEAM CONFIGURATIONS WITH DIFFERENT APPLIED TORQUES, $viii)\ \tau(t,s)=0, t>50$ AND $ix)\ \tau(t,s)=0, s>\frac{l}{2}$.

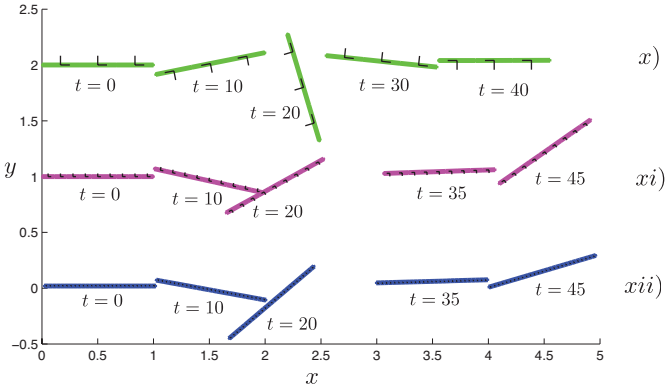

Figure 8. BEAM CONFIGURATIONS WITH DIFFERENT NUMBER OF ELEMENTS, *x*) $N = 3$, *xi*) $N = 9$ AND *xii*) $N = 27$. NO TORQUES ARE APPLIED ($A = 0$) AND THE BEAM IS GIVEN AN INITIAL VELOCITY $\boldsymbol{v}_0 = [10^{-1}, 10^{-4}]$ IN EVERY ELEMENT.

ating more than one percent of the beam's length from its initial value). Using $\mathbf{v}_0 = [0.1, \varepsilon]$ with $\varepsilon = 2.2 \cdot 10^{-16}$ being the floating-point relative accuracy in Matlab, and $N = 3$ (with 12 fluid panels per element), first unstable behavior was detected at $t = 35.13$. A slightly larger perturbation of the initial *y*-velocity $\mathbf{v}_0 = [0.1, 10^{-4}]$ lead to unstable motion at $t = 2.13$. The third considered initial velocity varies over the length of the beam according to $\mathbf{v}_0 = [0.1, (3.5 - \frac{s}{\Delta l}) \cdot 10^{-5}]$ and first deviations from the horizontal configuration occurred at $t = 3.8$.

Using $N = 9$ (with 4 panels per element) resulted in instability at $t = 78.1$, $t = 4.4$ and $t = 9.91$, for the different initial velocities, respectively. Simulations with 12 panels per element predicted unstable behavior at slightly earlier times, namely at $t = 78.03$, $t = 4.37$ and $t = 9.86$. Increasing the number of elements to $N = 27$, the influence of the number of fluid panels per element becomes negligible. First unstable behavior has been detected at $t = 82.04$, $t = 5.26$ and $t = 4.59$ for the different initial velocities. For all three discretizations, the behavior did not change when the bending stiffness varied with $EI \in \{5, 10, 10^2, 10^3, 10^4\}$.

Using the initial velocity $\mathbf{v}_0 = [0.1, 10^{-4}]$, Fig. 8 shows the motion of the coarsely discretized beam *x*) and the two finer discretizations in *xi*) and *xii*), respectively. On the one hand, it is visible that the coarse beam's behavior is very unstable – at $t = 10$, the beam has already rotated by almost 180^o. On the other hand one can observe that the behavior of the two finer beams does not differ significantly. These numerical experiments show that the onset of instability may be delayed by proper discretization of the beam. A rigorous analysis of the beam's stability, including its behavior in the continuous limit, remains to be undertaken in a future work.

7 CONCLUSIONS

The motion of a Cosserat beam submerged in an infinite volume of inviscid, incompressible fluid is proposed as a model for fish swimming. Due to the nonlinear coupling between the beam and the surrounding fluid (accounted for using the added mass effect), the submerged beam could undergo a net locomotion (swimming) subject to prescribed torsional loading on its centerline. Such loading can at most result in a net rotational motion in the absence of the fluid. In addition to the ability of the model to detect net displacements and rotations, it also accounts for the body's elastic effects, that is, deformations due to the prescribed loading. This is in contrast to the fish model presented in [3] which considers prescribed deformations and does not account for possible mechanical reflexes of the fish skin and muscles. The submerged beam model presented here provides a suitable framework for modeling fish swimming in a way that encodes the material properties of the fish and the shape actuation along its centerline. Indeed, properly modeling the elastic effects is indispensable for addressing issues related to the feasibility of a prescribed deformation in terms of the stresses and strains it causes in the fish body. Future extensions of this work will include more accurate models of the material behavior of the fish (better constitutive models) which will allow us to analyze the stresses and strains as well as the energy needed for locomotion in more detail.

REFERENCES

[1] Lighthill, J., 1975. *Mathematical Biofluiddynamics*. Society for Industrial and Applied Mathematics, PA.

[2] Wu, T., 1971. "Hydrodynamics of swimming fish and cetaceans". *Adv. Appl. Math.*, **11**, pp. 1–63.

[3] Kanso, E., Marsden, J., Rowley, C., and Melli-Huber, J., 2005. "Locomotion of articulated bodies in a perfect fluid". *Journal of Nonlinear Science*, **15**, pp. 255–289.

[4] Beal, D., Hover, F., Triantafyllou, M., Liao, J., and Lauder, G., 2006. "Passive propulsion in vortex wakes". *Journal of Fluid Mechanics*, **549**, p. 385402.

[5] Long, J., Hale, M., Mchenry, M., and Westneat, M., 1996. "Functions of fish skin: flexural stiffness and steady swimming of longnose gar, lepisosteus osseus". *J. Exp. Biol.*, **199**, p. 213951.

[6] Videler, J., 1993. *Fish Swimming*. Springer, New York.

[7] Wainwright, S., 2000. "The animal axis". *Am. Zool.*, **40(1)**, p. 1927.

[8] Cheng, J.-Y., J.Pedley, T., and Altringham, J. D., 1998. "A continuous dynamic beam model for swimming fish". *Philos. Trans. Royal Soc. London B*, **353**, pp. 981–997.

[9] Antmann, S., 1995. *Nonlinear Problems in Elasticity*. Springer.
[10] Simo, J., 1985. "A finite strain beam formulation. The three-dimensional dynamic problem. Part I". *Comput. Methods Appl. Mech. Engrg.*, **49**, pp. 55–70.
[11] Saffman, P. G., 1992. *Vortex Dynamics*. Cambridge University Press.
[12] Leyendecker, S., Betsch, P., and Steinmann, P., 2006. "Objective energy-momentum conserving integration for the constrained dynamics of geometrically exact beams". *Comput. Methods Appl. Mech. Engrg.*, **195**, pp. 2313–2333.
[13] Betsch, P., and Steinmann, P., 2002. "Frame-indifferent beam finite elements based upon the geometrically exact beam theory". *Int. J. Numer. Meth. Engng.*, **54**, pp. 1775–1788.
[14] Hess, J., and Smith, A., 1966. "Calculation of potential flow about arbitrary bodies". *Prog. Aeronaut. Sci.*, **8**, pp. 1–139.
[15] Katz, J., and Plotkin, A., 2001. *Low-Speed Aerodynamics*. Cambridge Aerospace Series, Cambridge.
[16] Moran, J., 1984. *An Introduction to Theoretical and Computational Aerodynamics*. John Wiley & Sons, New York.
[17] Marsden, J., and West, M., 2001. "Discrete mechanics and variational integrators". *Acta Numerica*, **10**, pp. 357–514.
[18] Leyendecker, S., Marsden, J., and Ortiz, M., 2008. "Variational integrators for constrained dynamical systems". *ZAMM*, **88**(9), pp. 677–708.